Geoderma 428 (2022) 116217

Contents lists available at ScienceDirect

Geoderma

journal homepage: www.elsevier.com/locate/geoderma

Iron speciation changes and mobilization of colloids during redox cycling in Fe-rich, Icelandic peat soils

Laurel K. ThomasArrigo *, Ruben Kretzschmar

Soil Chemistry Group, Institute of Biogeochemistry and Pollutant Dynamics, Department of Environmental Systems Science, ETH Zurich, Universitätstrasse 16, CHN, CH-8092 Zurich, Switzerland

ARTICLE INFO

Handling Editor: Daniel Said-Pullicino

Keywords:
Iceland
Iron biogeochemistry
Organic carbon
Colloids
Wetlands

ABSTRACT

Soils of Iceland are characterized by an abundance of short-range order (SRO) iron (Fe) minerals and aluminosilicates. Interactions between these SRO mineral phases and soil organic carbon (OC) promote long-term stabilization of the latter through the formation of mineral-organic complexes and aggregates. However, Icelandic soils are also exposed to high rainfall events, which induce anoxic conditions, facilitate microbial reduction of ferric Fe, and may lead to the mobilization of mineral-associated OC. Here, we explored the fate of OC during Fe redox cycling by incubating six organic-rich soil horizons from three typical soil types across Iceland (Histosols, Histic and Gleyic Andosols) as soil slurries under anoxic conditions for up to 5 weeks and followed the effects of re-oxidation after 1, 2, and 5 weeks. Changes in solid-phase Fe speciation were assessed by combining Fe *K*-edge X-ray absorption spectroscopy with time-resolved parallel selective chemical extractions, and trends in aqueous element contents were measured in both the dissolved (<3 kDa) and fine colloidal fractions (3 kDa to 0.45 μm). In all soils, anoxic incubation resulted in microbial reduction of Fe(III) and concomitant increases in soil solution pH. However, soils containing SRO Fe minerals underwent more extensive Fe reduction. Rapid (<1 wk) increases in aqueous element contents (including Fe, Al, and OC) were recorded in all soil slurries, and mobilization of colloids occurred in soil horizons which reached the highest pH values (>4.6). Mobilized colloids persisted during re-oxidation of the soil slurries, which also resulted in the formation of new Fe mineral phases, the composition of which was influenced by initial soil Fe mineralogy. Collectively, our results suggest that increases in the frequency of redox cycles in Icelandic soils are likely to result in shifts in Fe mineralogy and may contribute to the increased mobilization of soil OC as organic-Fe-/Al-colloids.

1. Introduction

Volcanic soils (Andosols) account for <2 % of the global land area, yet store up to 5 % of global soil organic carbon (SOC) (Eswaran et al., 1993). This is due, in part, to the abundance of reactive, short-range order (SRO) iron (Fe) minerals and aluminosilicates characteristic of Andosols (WRB, 2014). With high specific surface areas, SRO Fe minerals (e.g., ferrihydrite; $Fe_{10}O_{14}(OH)_2{\cdot}mH_2O$, nanogoethite; α-FeOOH) and aluminosilicates (e.g., allophane; $Al_2O_3{\cdot}(SiO_2)_{1.3\text{-}2}{\cdot}(2.5\text{–}3)H_2O$, imogolite; $Al_2SiO_3(OH)_4$) facilitate the sorption and occlusion of organic carbon (OC) in mineral-aggregate structures, hindering its biodegradation and mineralization (Gu et al., 1994; Lalonde et al., 2012; Torn et al., 1997). However, under reducing conditions, ferric iron (Fe(III)) acts as a terminal electron acceptor for microorganisms during anaerobic respiration of OC (Melton et al., 2014). Electron transfer induces reductive dissolution, recrystallization, or transformation of Fe minerals (Handler et al., 2014; Hansel et al., 2005), leading to the mobilization of associated OC as dissolved organic carbon (DOC) (Bhattacharyya et al., 2018) or in organic-Fe-/Al-colloids (Buettner et al., 2014; Thompson et al., 2006a), which may be subsequently mineralized (Bhattacharyya et al., 2018), form stable complexes with dissolved Fe (Daugherty et al., 2017), be transported to deeper soil horizons (Marin-Spiotta et al., 2011), or contribute to the overall export of OC and Fe from terrestrial to aquatic systems.

In general, mountainous volcanic islands contribute significantly to the particulate suspended matter released to the oceans (Lloret et al., 2011; Milliman and Syvitski, 1992). Thus, recent years have seen an increased motivation to understand SOC mobilization coupled to Fe biogeochemistry in volcanic soils. By and large, these studies have considered Fe redox cycling in mineral and organic horizons of tropical

* Corresponding author.
E-mail address: laurel.thomas@usys.ethz.ch (L.K. ThomasArrigo).

https://doi.org/10.1016/j.geoderma.2022.116217
Received 5 August 2022; Received in revised form 3 October 2022; Accepted 7 October 2022
Available online 23 October 2022

volcanic island soils (Barcellos et al., 2018; Bhattacharyya et al., 2018; Chen et al., 2018; Coward et al., 2018; Coward et al., 2017; Dubinsky et al., 2010; Ginn et al., 2017; Hall and Silver, 2013; Thompson et al., 2006a; Thompson et al., 2006b; Wilmoth et al., 2018) and collectively suggest that soil Fe mineral content, the rate and duration of oxidation/reduction cycles, and the trajectory of Fe mineral transformations during redox cycling (e.g., from poorly- to highly-crystalline or vice versa) are critical factors influencing SOC mobilization. In contrast to examples of well-studied tropical volcanic island soils, the coupled biogeochemical cycling of Fe and C in high latitude Andosols, like those found throughout Iceland, the Kamchatka peninsula (Russia), and regions in Alaska, is less understood. However, these soils are highly relevant as changing climate patterns are expected to disproportionately impact high latitudes (Bekryaev et al., 2010; Hinzman et al., 2013; Stocker et al., 2013). Incipient warming will increasingly degrade permafrost and intensify evapotranspiration; thus modifying soil drainage regimes, river discharge, and the frequency of redox cycles in near-surface soils (Hinzman et al., 2005; Hinzman et al., 2013; Rawlins et al., 2010; Smith et al., 2005). Because SRO Fe minerals are prone to rapid reductive dissolution (Roden and Zachara, 1996), climate change and associated shifts in hydrologic regimes are likely to influence Fe redox cycling in high latitude Andosols, consequently impacting the storage and mobility of mineral-associated SOC.

Iceland is a volcanic island situated between the 63rd and 66th parallel north. In addition to SRO-mineral rich Andosols, Iceland has an abundance of organic-rich Histosols, the development of which is promoted by the generally mild winters and cool summers (mean annual temperature is 0-4° C below 200 m) and short growing season (3–5 months), which result in low rates of organic matter decomposition (Arnalds, 2015). Soil organic carbon accumulation in Icelandic Histosols is additionally aided by the high SRO-mineral content, arising from the rapid weathering of basalt minerals and high rates of aeolian deposition of Fe-rich (~10 wt%) volcanic glass (ranging from 10 to >250 g m^{-2} yr^{-1} depending on location) (Arnalds, 2010). Collectively, the climate of Iceland and the andic properties of its soils promote the storage of an estimated 2.1 Pg of SOC (Óskarsson et al., 2004), much of which is found in the ~9000 km^2 of minerotrophic wetlands which account for 19 % of Iceland's vegetated land surface (Arnalds et al., 2016). However, Iceland is also subject to moderate to high annual rainfall (from <400 to >4500 mm yr^{-1} depending on location) and occasionally intense rainfall events (>100 mm day^{-1}) (Arnalds, 2015; Ólafsson et al., 2007) which may lead to perdiodic flooding of surface soils and facilitate redox cycling in upper soil horizons. Considering the current precipitation rates and the anticipated shifts in hydrologic regimes due to climate change, understanding Fe biogeochemistry as it relates to SOC mobilization in these soils is critical to predicting regional to global biogeochemical cycling of Fe and C in the context of changing climate.

The combination of organic soils with high mineral content, the continual replenishment of poorly-weathered volcanic material via aeolian deposition, and the generally cool and short growing season renders Icelandic soils uniquely different compared to the well-studied tropical volcanic island soils. Thus, it seems likely that factors controlling the biogeochemical cycling of Fe and C in these soils may differ as well. Therefore, in this study, we aimed to present the first data on the Fe redox cycling coupled to SOC mobilization as DOC (<3 kDa) and in colloids (3 kDa to 0.45 μm) in Fe- and organic-rich Icelandic soils. To this end, we selected soils from three typical soil types across Iceland with contrasting properties representing range of aeolian deposition rates (10–50, 20–100, and 75–250 g m^{-2} yr^{-1}), mean annual precipitation (~400, ~1000, and ~1400 mm yr^{-1}), and soil classification (Histosol, Histic and Gleyic Andosol). From these soils, we then chose six organic-rich subsoil horizons demonstrating a range of C:Fe molar ratios (8.1–74) to be included in an oxic/anoxic incubation study. Soil slurries were subjected to reducing conditions for up to 5 weeks with the effects of re-oxidation examined after 1, 2, and 5 weeks. We followed changes in solution geochemistry, including Eh and pH, and measured total element concentrations in both dissolved (<3 kDa) and colloidal (3 kDa to 0.45 μm) fractions. Coupled to changes in solid-phase Fe speciation, determined through parallel selective chemical extractions and Fe *K*-edge X-ray absorption spectroscopy, the results show that the fate of Fe and C during redox cycles is affected by both inherent soil mineralogy as well as geochemical parameters of the soil solution.

2. Materials and methods

2.1. Environment and site descriptions

The parent materials of most Icelandic soils are volcanic and soil development is largely affected by rates of aeolian deposition of volcanic ash and soil drainage conditions (Arnalds, 2004). The former is primarily controlled by proximity to dust sources, with high aeolian deposition rates nearer to active volcanic belts limiting soil development and lower deposition rates and the distribution of finer material found with increasing distances from dust sources (Arnalds, 2015). Soil drainage conditions are affected by the regional bedrock. While the permeability of younger bedrock near the active volcanic belts is high, the older Tertiary basalts, found throughout the north, northwest, and eastern parts of Iceland, exhibit lower permeability due to weathering, alterations, and the formation of secondary minerals which fill pore spaces in the Tertiary rocks, resulting in slower drainage conditions. Combined, these factors lead to the formation of weakly developed, non-vegetated soils (Vitrisols and Leptosols) nearer to the active volcanic belts and to increasingly organic soils (Andosols and Histosols) forming with increasing distance from dust sources (Arnalds, 2015). Altogether, Iceland soils comprise 44 % Vitrisols and Leptosols, 54 % Andosols (Brown, Gleyic and Histic), and 1 % Histosols (Arnalds, 2004). It should be noted that these terms are based on the Icelandic soil classification system, which differentiates soil type based on C content in the upper 30 cm (>20 % C = Histosol; 12–20 % C = Histic Andosol; <12 % C, gleying/mottles = Gleyic Andosol; <12 % C, dry = Brown Andosol) (Arnalds, 2004).

For this study, four soils from three typical soil types across north and western Iceland were selected (Figure S1). All sites are relatively flat, poorly drained wetland soils covered in grasses and are typical examples of drainage-impacted low lying (<200 m elevation) wetlands (Arnalds, 2015). The soils; two Histosols (Hestur_H and Hindisvik_H), a Histic Andosol (Selfoss_HA) and a Gleyic Andosol (Hestur_GA), were named after the Icelandic soil classification system (Table 1) (Arnalds, 2004). Soils at the Hindisvik site, on the northern tip of the Vatnsnes peninsula, are developed on Tertiary basalt (Harðarson et al., 2008), and receive the lowest amount of aeolian deposition (10–50 g m^{-2} yr^{-1}) (Arnalds, 2010) and have the lowest mean annual precipitation (MAP) (389 mm yr^{-1}) and the lowest mean annual temperature (MAT) (3.9 °C), (station Blönduós, 2004–2020; Iceland Meteorological Office, IMO). Thus, Hindisvik represents the coldest, driest site with the lowest aeolian influx. In 2019 (the year of sampling), the MAT was 3.7 °C and specific annual precipitation was slightly higher than average (433 mm yr^{-1}). Recently, the mineral and elemental composition of Fe-rich organic precipitates sampled from drainage ditches directly next to the Hindisvik_H soil profile were characterized (ThomasArrigo et al., 2022).

The two Hestur sites are located within the Borgarfjörður catchment. Previously, nutrient cycling and weathering processes of soils in this area have been studied using elemental and isotope composition analyses (Opfergelt et al., 2014; Opfergelt et al., 2017), while rivers in the Borgarfjördur catchment have been the focus of multiple studies reporting the chemical and isotope composition of dissolved and suspended river materials relating to weathering processes (e.g., Georg et al., 2007; Hawley et al., 2017; Hindshaw et al., 2013; Pogge von Strandmann et al., 2008). Characterization of Fe-rich organic precipitates from the drainage ditches near the Hestur_GA profile was likewise included in a recent study (ThomasArrigo et al., 2022). Basalts from western Iceland in the Borgarfjörður catchment are primarily

Table 1
Location of the selected soil profiles and site description information.

Site Name	Soil type[a]	Soil type[b]	Latitude N	Longitude W	Elevation (m.a.s.l.)	MAT[c] (°C)	MAP[d] (mm yr^{-1})	Aeolian deposition rate (g m^2 yr^{-1})
Hestur_GA	Gleyic Andosol	Vitric Andosol	64°33′48.38″	21°30′20.27″	42	4.6	988	20–100
Hestur_H	Histosol	Andic Histosol	64°34′27.27″	21°35′42.68″	46	4.6	988	20–100
Selfoss_HA	Histic Andosol	Vitric Andosol	63°54′43.91″	20°59′45.42″	11	5.2	1434	75–250
Hindisvik_H	Histosol	Andic Histosol	65°39′2.75″	20°45′2.12″	26	3.9	389	10–50

[a] After the Icelandic soil classification system (Arnalds, 2004).
[b] After the WRB (WRB, 2014).
[c] Mean annual temperature.
[d] Mean annual precipitation.

Tertiary (older than 3.1 Ma) (Harðarson et al., 2008). With an aeolian deposition rate of 25–100 g m^{-2} yr^{-1} (Arnalds, 2010), MAP of 988 mm yr^{-1} and MAT of 4.6 °C (station Hvanneyri, 2002–2020; IMO), the Hestur site represents an intermediate site in all terms. In 2019, MAT was 4.7 °C and specific annual precipitation was slightly lower than average (747 mm yr^{-1}).

Compared to the Hestur and Hindisvik sites, the Selfoss site, located ca. 2 km south of the town of Selfoss, receives the highest influx of aeolian deposition (75–250 g m^{-2} yr^{-1}) (Arnalds, 2010) and also receives the most precipitation (MAP is 1434 mm yr^{-1}) and is slightly warmer than the other sites (MAT is 5.3 °C) (station Eyrarbakki, 2003–2016; IMO). In 2019, the MAT was 5.2 °C and specific annual precipitation was not reported. In this area, geology is dominated by Plio-Pleistocene bedrock and post-glacial lava flows (0.8 – 3.3 Ma) (Harðarson et al., 2008).

2.2. Soil sampling and characterization

Soils for characterization and incubation studies were collected in June 2019. Soil profiles were described following FAO guidelines (WRB, 2014). All soil profiles were prepared from the walls of drainage ditches already existing within the wetlands. Therefore, all soils were described, collected and stored under oxic conditions. Individual horizons were manually homogenized and packaged in their field-moist state into plastic bags which were then stored at 4 °C in the dark. Subsets of each soil horizon were air dried (30 °C) and sieved (<2 mm, nylon) for characterization. Soil pH was determined after re-suspending the dried soil in ultrapure water (UPW, Milli-Q®, Millipore, 18.2 MΩ·cm) at a solid:solution ratio of 1:5 for 1 hr. Total element contents of each soil horizon were measured with energy-dispersive X-ray fluorescence (XRF) spectrometry (Spectro X-Lab 2000) and total C and N contents with an elemental analyzer (Vario MAX Cube, Elementar).

Mineral composition of the soil horizons was determined by powder X-ray diffraction (XRD, D8 Advance, Bruker). For these analyses, dried and sieved soil samples were milled to ~ 50 μm using a disk swing mill. Milled sample material was analyzed as powder XRD in Bragg − Brentano geometry using Cu $K\alpha_{1,2}$ radiation (λ = 1.5418 Å, 40 kV, and 40 mA) and a high-resolution energy-dispersive 1-D detector (LYNXEYE). Diffractograms were recorded from 10° to 70°2θ with a step size of 0.02°2θ and 6 s acquisition time per step. For the soil horizons selected for use in this soil incubation study, the relative contributions of the crystalline mineral phases in the diffraction patterns were determined by Rietveld Quantitative Phase Analysis (QPA) using the TOPAS software (Version 5, Bruker AXS) in combination with published crystallographic structure files. Crystallite sizes were estimated by fitting the sample peak broadening with the Cry size L parameter in TOPAS based on the Double-Voigt Approach and are reported as LVol-IB, taking instrumental broadening into account using LaB_6 powder (NIST Standard Reference Material 660c, mean volume-weighted domain size 0.8 μm) as reference material. Additionally, the amounts of amorphous materials were estimated by the internal standard method in the TOPAS software using aluminum oxide (Al_2O_3, Fluka) as the internal standard mixed into the soil at a mass ratio of 1:2 (Al_2O_3:soil).

2.3. Soil slurry incubation.

Prior to starting the experiment, the field-moist soils selected for the incubation were sieved to <2 mm and visible plant or root material was removed with tweezers. The prepared soils were then packaged into plastic bags and kept at 25 °C in the dark for two weeks to allow soil microorganisms to recover from 4 °C storage. Soil incubations were performed in triplicates as soil slurries at a soil:water ratio of 1:10 in the dark at 25 °C in a temperature-controlled room. Field-moist soils (11–21 g, 4.5 g dry mass equivalent) were weighed into Al-wrapped 117 mL septum bottles and re-suspended in fresh UPW (24–34 mL). Septum bottles were then covered in Parafilm and set on an orbital shaker (150 rpm) at 25° C. To establish conditions at the start of the incubation, after 2 h subsets of the incubation bottles (in triplicates) were sacrificially sampled. To this end, pH and Eh were measured directly in the soil slurry and oxic aqueous samples were collected as described below.

The remaining septum bottles were then crimp-sealed with a rubber stopper and Al cap and the headspace of the bottles was purged with N_2 gas at a flow rate of 750 mL min^{-1} for 5 min. The soil slurries were then returned to the orbital shaker. After 1, 2, and 5 weeks, subsets of the incubation bottles (in triplicates) were moved into an anoxic glovebox (N_2 atmosphere, <1 ppm (v/v) O_2, MBRAUN) where they were opened for sacrificial anoxic sampling. First, pH and Eh were measured directly in the soil slurry. The bottles were then manually agitated to ensure re-suspension of all soil particles, and half of the soil slurry (~22 mL) was poured into 50 mL Falcon tubes, which were capped, wrapped in Parafilm, and removed from the glovebox for centrifugation (MSE Mistral 6000). To assess the formation and mobilization of colloids during Fe redox cycles, we considered two particle size cut-offs; <0.45 μm and <3 kDa, with the latter representing the truly dissolved phase. The calculated difference between element concentrations passing these filter cutoffs is defined here as the fine colloidal fraction (3 kDa to 0.45 μm). To this end, the Falcon tubes were centrifuged for 10 min at 3000 rpm (ca. 2500*g*) to obtain a theoretical particle size fraction of <0.45 μm. Centrifuge times were calculated from Stoke's law assuming a spherical particle geometry and a nominal particle density of 1.65 g cm^3; a value which has been previously been determined and used for organic-rich volcanic soils (Buettner et al., 2014; Marin-Spiotta et al., 2011). However, following the 10 min centrifugation, some larger organic particles remained in suspension. Therefore, centrifuged tubes were returned to the glovebox and an aliquot of the supernatant was decanted and additionally filtered (<0.45 μm, nylon) and acidified for further aqueous analyses (described in Section 2.4). The remaining supernatant was pipetted off and transferred into 15 mL Ultracel® 3 K centrifuge tubes (Amicon® Ultra-15, PLC membrane, 3000 MWCO, Merck) for ultracentrifugation. The ultracentrifuge tubes were similarly capped, wrapped in Parafilm, and removed from the glovebox for centrifugation (3000*g*, 15 min). After centrifugation, the ultrafiltrates were then returned to the glovebox and acidified for further aqueous analyses (described in Section 2.4). Immediately prior to use, the Ultracel® 3 K centrifuge tubes were pre-rinsed with 15 mL of 0.1 M NaOH followed by 15 mL of UPW (3000*g*, 15 min each) to remove potential traces of glycerine.

Following centrifugation and decanting, the residual solid-phase was manually shaken and re-suspended in 10 mL of anoxic UPW. The Falcon tubes were then again capped, wrapped in Parafilm, and removed from the glovebox for centrifugation (3000*g*, 30 min), after which the tubes were opened (in ambient air), the supernatant rapidly decanted, and the residual solid-phase was immediately flash-frozen in N_2(l) and freeze-dried. Immediately afterwards, tubes were returned to the glovebox where triplicate solid-phase residuals were combined, manually homogenized, and stored in the dark until further analyses.

Following the anoxic sampling described above, the Al-wrapped septum bottles still containing the remaining half of the soil slurry (~22 mL) were removed from glovebox, sealed in Parafilm to allow gas exchange but prevent evapotranspiration, and returned to the orbital shaker (150 rpm) at 25 °C. The soil slurries were allowed to oxidize for 2, 4, or 8 days (following 1, 2, or 5 week anoxic incubation times, respectively), after which time Eh and pH measurements and aqueous- and solid-phase sampling was performed as described above, however this time entirely under ambient air conditions.

2.4. Aqueous phase analyses

To follow the mobilization of trace elements and nutrients during soil flooding and re-oxidation, aqueous samples, both <0.45-μm and <3 kDa filtrates, were analyzed for aqueous OC and nitrogen (DIMA-N coupled to a Dimatoc 2000 TOC analyzer, Dimatec) and total element contents (with inductively coupled plasma-optical emission spectrometry; ICP-OES, Agilent 5100, and inductively coupled plasma-mass spectrometry; ICP-MS, Agilent 8800 Triple Quad). Aqueous Fe speciation (Fe (total) and ferrous Fe (Fe(II))) was measured in the 5 week anoxic samples with the 1,10-phenanthroline method (Loeppert and Inskeep, 1996), whereby Fe(II) was determined after an excess of nitriloacetic acid was added to mask the Fe(III) (Fadrus and Malý, 1975).

2.5. Selective chemical extractions

To estimate the amount of Fe in various chemical forms prior to and during redox cycles, we performed selective chemical extractions in parallel to target total reactive Fe not bound in silicates (dithionite-citrate extraction (Holmgren, 1967); 'D'), the amount of 'organically-bound or colloidal Fe' (Na-pyrophosphate (McKeague, 1967); 'P'), and the amount of Fe in poorly-crystalline or amorphous mineral form (acid ammonium oxalate extraction (Loeppert and Inskeep, 1996); 'O'). For the dithionite-citrate extraction, ~200 mg of 2 mm-sieved, homogenized, dried soil material was weighed into 50 mL Falcon tubes to which 12.5 mL of 0.57 M sodium citrate solution and 0.2 g of sodium dithionite powder were added. The tubes were then shaken (end-over-end) for 16 h in the dark. For the Na-pyrophosphate treatment, ~100 mg of 2 mm-sieved, homogenized, dried soil material was weighed into 50 mL Falcon tubes to which 10 mL of 0.1 M Na-pyrophosphate solution was added. The suspensions were shaken (end-over-end) for 16 h in the dark. For the acid ammonium oxalate extraction, ~250 mg of 2 mm-sieved, homogenized, dried soil material was weighed into 50 mL Falcon tubes to which 10 mL of a 0.2 M ammonium oxalate solution in 4:3 ratio with oxalic acid (pH 3) was added. The suspensions were shaken (end-over-end) for 4 h in the dark. For all extractions, following the end-over-end shaking, the suspensions were centrifuged (3500*g*, 40 min) and filtered (<0.45 μm, nylon). Element concentrations in the filtered extracts were determined with ICP-OES. All solid-phase chemical extractions were performed in duplicates and the values reported are the average.

2.6. Fe K-edge X-ray absorption spectroscopy

Speciation of solid-phase Fe in the soil horizons prior to, after 5 weeks of flooded incubation, and following subsequent oxidation was analyzed by bulk Fe *K*-edge (7112 eV) X-ray absorption spectroscopy (XAS) at the LUCIA and SAMBA beamlines of SOLEIL (Saint-Aubin, France) and at the XAFS beamline of ELETTRA (Trieste, Italy). For these measurements, dried unreacted and reacted soil material was manually homogenized with a mortar and pestle until all material passed a <350 μm sieve and then was pressed into 10 mm pellets and sealed with Kapton® tape. At the LUCIA beamline, X-ray absorption near the edge structure (XANES) and extended X-ray absorption fine structure (EXAFS) spectra were recorded in transmission mode at ~70 K using a He(l) cryostat. Higher harmonics in the beam were eliminated by mirrors. Three to four scans per sample were collected and averaged. At the SAMBA beamline, transmission spectra were recorded in continuous scan mode at ~80 K using a N_2(1) cryostat. Higher harmonics in the beam were eliminated by mirrors. Ten to fifteen scans were collected and averaged. At the XAFS beamline, spectra were recorded in transmission mode at ~80 K using a N_2(l) cryostat. Higher harmonics in the beam were eliminated by detuning the monochromator by 30 % of its maximal intensity and two to four scans were collected and averaged. Monochromators at each beamline (Si(1 1 1) at LUCIA and XAFS, Si (2 2 0) at SAMBA) were calibrated to the first-derivative maximum of the *K*-edge absorption spectrum of a metallic Fe foil (7112 eV). The foil was continuously monitored to account for small energy shifts (<1 eV) during the sample measurements.

All spectra were energy calibrated, pre-edge subtracted, and post-edge normalized in Athena (Ravel and Newville, 2005). Linear combination fit analyses of Fe *K*-edge XANES spectra were conducted over an energy range of −20 to 30 eV (E-E_0) with E_0 of sample and reference compound spectra defined as zero-crossing in their second XANES derivatives. Linear combination fit analyses of k^3-weighted Fe *K*-edge EXAFS spectra were performed over a *k*-range of 2–12 $Å^{-1}$ with the E_0 of all spectra and reference compounds set to 7128 eV. No constraints were imposed during LCF analyses, and initial fit fractions (XANES: 104 ± 3 %, EXAFS: 94 ± 11 %) were recalculated to a compound sum of 100 %. Iron reference compounds for LCF analysis were selected after principal component analysis and target-transform testing (PCA-TT, Tables S6 and S7). Further details to PCA-TT and LCF analyses are found in the Supporting Information.

3. Results

3.1. Soil profile descriptions and (iron) mineralogy

Selected physical and chemical characteristics of the soil profiles at each site are presented in Table S1. All profiles contained horizons that were rich in organic C (23 ± 14 wt% C, $\bar{x} \pm \sigma$) and C content generally increased with depth. Ratios of C/N ranged between 13 and 22 ($\bar{x} = 16$). Only the Hestur_GA profile comprised alternating layers of organic (>20 wt% C) (WRB, 2014) and mineral soil horizons with low C content (2.6 ± 1.4 wt% C). A thin light-colored tephra layer was observed in the Hindisvik_H profile at 40–42 cm depth, consistent with deposition of rhyolitic tephra material. All soils were slightly acidic (pH = 5.1 ± 0.9), with the lowest values measured in horizons of the Hindisvik_H profile (pH = 3.08 to 5.34) and the highest values measured in the Hestur_GA profile (pH = 5.10 to 6.40). The relatively high C contents, C/N ratios, and slightly acidic pH of the soil profiles are consistent with descriptions of other poorly drained soils in Iceland (Arnalds, 2015; Arnalds et al., 2016; Opfergelt et al., 2014; Opfergelt et al., 2017). Yet, overall C contents are generally lower than those reported from other arctic and boreal wetland soils (Arnalds et al., 2016) and reflect the high mineral content of Icelandic Andosols and Histosols.

Total Fe content (Fe_T) of the soils varied between 25 and 210 mg g^{-1} ($\bar{x} = 71$), total reactive Fe not bound in silicates (Fe_D) accounted for 47 ± 46 % of Fe_T and the amount of Fe in poorly-crystalline or amorphous mineral form (Fe_O) accounted for 43 ± 21% of Fe_T. Organically-bound or colloidal Fe (Fe_P) accounted for 30 ± 19 % of Fe_T. While Fe_T was higher in the Hestur soils (Hestur_GA and Hestur_H) than in the Hindisvik_H profile, all three soils showed similarly high amounts of extractable Fe compared to the lower total and extractable Fe contents in

the Selfoss_HA profile. The fraction of acid ammonium oxalate extractable Fe compared to total reactive Fe not bound in silicates (e.g., Fe_O/Fe_D) is often used as an indicator of the degree of soil development in volcanic soils (Malucelli et al., 1999). However, in agreement with reported Fe_O/Fe_D ratios in other Icelandic soil profiles (Bonatotzky et al., 2019, 2021; Opfergelt et al., 2014), the ratio of Fe_O/Fe_D in the soils studied here ranged from 0.3 to 5.8 ($\bar{x} = 1.4$, Table S1); relatively high values indicating a high fraction of poorly-crystalline material throughout the soil profiles. Alternatively, significantly higher amounts of Fe_O compared to Fe_D may the indicate the structural incorporation of Fe into poorly crystalline aluminosilicates (Baker et al., 2014) or the occlusion of ferrihydrite nanoparticles within allophane aggregate structures (Filimonova et al., 2016), as, in contrast to acid ammonium oxalate, dithionite-citrate may weaken the allophane or imogolite structures however is not expected to completely dissolve the mineral phases (Dahlgren, 1994) (compare Al_D and Al_O, Table S1). Allophane content of the soils, estimated as $6*Si_O$ (Parfitt, 1990), ranged from 0.3 to 9.3 % ($\bar{x} = 3.1$), but was mostly <6 %; a cut-off used to distinguish between Brown and Gleyic Andosols in the Icelandic soil classification system (Arnalds, 2015). Highest allophane contents were found in the higher pH soil horizons of Hestur_GA, as the formation of allophane is favored at pH >5; below pH 5 metal-humus complex formation is favored (Parfitt and Kimble, 1989). In agreement, allophane contents were lowest in the low pH soil horizons of Hindisvik_H.

The main chemical properties of the organic soil horizons selected for this incubation study are summarized in Table 2. All soil horizons used in the incubation experiments were slightly acidic (pH = 3.08 to 6.10) and had high C contents (from 21 to 43 wt% C). Organic matter in each of the horizons could be described as poorly-decomposed fibrous material, in agreement with previous descriptions of organic matter in Icelandic wetland soils (Arnalds, 2015). However, soil horizons varied in both Fe_T (from 27 to 122 mg g^{-1}) as well as fractions of Fe_D (15 to 59 % of Fe_T), Fe_O (17 to 89 % of Fe_T) and Fe_P (8 to 59 % of Fe_T), resulting in a range of C:Fe molar ratios (C_T:Fe_T = 8.1 to 74).

X-ray diffraction patterns of all soil horizons are shown in Figures S2-S5 and results from QPA fits from the soil horizons used in the incubation experiments are detailed in Table S3. Although evidence from selective chemical extractions suggests the presence of short-range ordered phases like ferrihydrite, allophane, and/or imogolite in each of the soil horizons, the presence of additional amorphous materials (e.g., amorphous Si) is similarly plausible, in addition to amorphous organic matter. Indeed, the amorphous fraction of all soil horizons included in this incubation study was ≥80 % (Table S3). Therefore, despite presence of amorphous features visible in XRD patterns of many of the soil horizons, some of which seem to correspond to ferrihydrite (visible as broad maxima around 2.54 and 1.49 Å or ~35 and ~62 °2θ), mineralogy of only the crystalline fraction in the soils was quantitatively assessed through QPA of XRD patterns. The crystalline mineral fraction of all soil horizons studied here comprised plagioclase (mostly anorthite) and pyroxenes (mostly augite), with small contributions from quartz (≤2.5 %), while soil horizons from the Hestur_H site additionally contained significant amounts of nanocrystalline goethite (56–64 %), with estimated crystallite sizes of <10 nm.

3.2. Trends in aqueous geochemistry during reducing periods

At the start of the incubation (2 h timepoint), measured Eh and pH of the soil slurries already showed variations (Fig. 1, left panel), with Eh values ranging from +418 to +708 (in Hestur_GA_45-60 and Hindisvik_H_70-100, respectively) and pH ranging from 2.95 to 5.70 (in Hindisvik_H_70-100 and Hestur_GA_75-90, respectively). Over the course of the incubation, the measured redox potential steadily decreased in all soil slurries, resulting Eh values ranging from −58 ± 4 (Hestur_GA_75-90) to 288 ± 11 (Hestur_H_82-130) after 5 weeks. The drop in redox potential was accompanied by concomitant increases in pH in all soil slurries (Fig. 1, left panel). After five weeks, the highest shifts in pH were recorded for Hestur_GA_45-60 and Hindisvik_H_70-100 (1.84 and 1.5 pH units, respectively) followed by Hestur_GA_75-90 (1.25 pH units) and Hestur_H_41-82 and Selfoss_HA_40-90 (both 0.67 pH units). Hestur_H_82-130 showed pH increases of <0.3 pH units.

All soils showed increases in aqueous Fe concentrations over the course of the incubation (Fig. 1, middle panel). After 5 weeks, the highest amounts of aqueous Fe in solution were recorded for Hindisvik_H_70-100, with 174 mmol kg^{-1} in the <0.45-μm fraction, which accounts for nearly 10 % of total soil Fe (compare to Fe_T, Table 2). High amounts of aqueous Fe in the <0.45-μm fraction were also recorded for Hestur_GA_45-60 (54.8 mmol kg^{-1}, 4.8 % of Fe_T), while lower amounts of aqueous Fe (<15.5 mmol kg^{-1}, <2 % of Fe_T) were measured for all other soils. For most soils, aqueous Fe in the dissolved fraction (<3 kDa) increased at a slower rate compared to the <0.45-μm fraction, suggesting the mobilization of Fe in colloids (e.g., the fraction between 3 kDa and <0.45 μm). In contrast, significantly less colloidal Fe was released from Hestur_H_82-130 and Hindisvik_H_70-100, as seen in the similar amounts of aqueous Fe in both the <3 kDa and <0.45-μm fractions at all timepoints during the incubation, despite similar (Hestur_H_82-130) or significantly higher (Hindisvik_H_70-100) total aqueous Fe concentrations. Similar trends in total aqueous elements, including the mobilization of elements in colloids in all soils except for Hestur_H_82-130 and Hindisvik_H_70-100, are shown for Al, Mn, Si, Mg, Ca, N, S, and P in Figures S7-S9. For all soils, aqueous Fe speciation, determined in the 5-week incubated aqueous samples, confirmed that Fe (II) accounted for the majority of Fe species in both the <0.45-μm and <3 kDa fractions (89 ± 10 % and 94 ± 5 %, respectively).

Mirroring trends in aqueous Fe, amounts of aqueous OC in solution increased in all soils during the incubation (Fig. 1, right panel). After 5 weeks of anoxic incubation, amounts of aqueous OC in the <0.45-μm

Table 2
Main characteristics of organic soil horizons included in this study.

Site Name	Depth[a]	pH	C_T	Fe_T[c]	Al_T[c]	Si_T[c]	C:Fe	C:N	Fe_D[d]	Fe_O[e]	Fe_P[f]
	(cm)	(H_2O)[b]	(mg g^{-1})	(mg g^{-1})	(mg g^{-1})	(mg g^{-1})	(mol/mol)	(mass ratio)	(mg g^{-1})	(mg g^{-1})	(mg g^{-1})
Hestur_GA	45–60	5.10	270	63	27	66	19.8	16.3	31.2	31.7	22.8
	75–90	6.10	211	122	21	64	8.1	18.2	35.2	74.3	9.7
Hestur_H	41–82	5.02	212	85	43	58	11.6	16.1	50.5	14.2	35.5
	82–130	4.26	432	27	17	14	74	19.8	14.8	11.0	9.5
Selfoss_HA	40–90	5.78	251	29	41	77	40	16.4	4.4	8.4	4.9
Hindisvik_H	70–100	3.08	363	90	03	11	18.6	17.7	13.9	80.0	53.1

[a] Below soil surface.
[b] Measured in suspended soils (1:5 solid:solution ratio) after 1 h at room temperature.
[c] Element totals, measured with XRF.
[d] Dithionite-citrate extraction (Holmgren, 1967).
[e] Acid ammonium oxalate extraction (Loeppert and Inskeep, 1996).
[f] Sodium-pyrophosphate treatment (McKeague, 1967). Additional parameters and information to the remaining soil horizons of each profile are presented in Table S1.

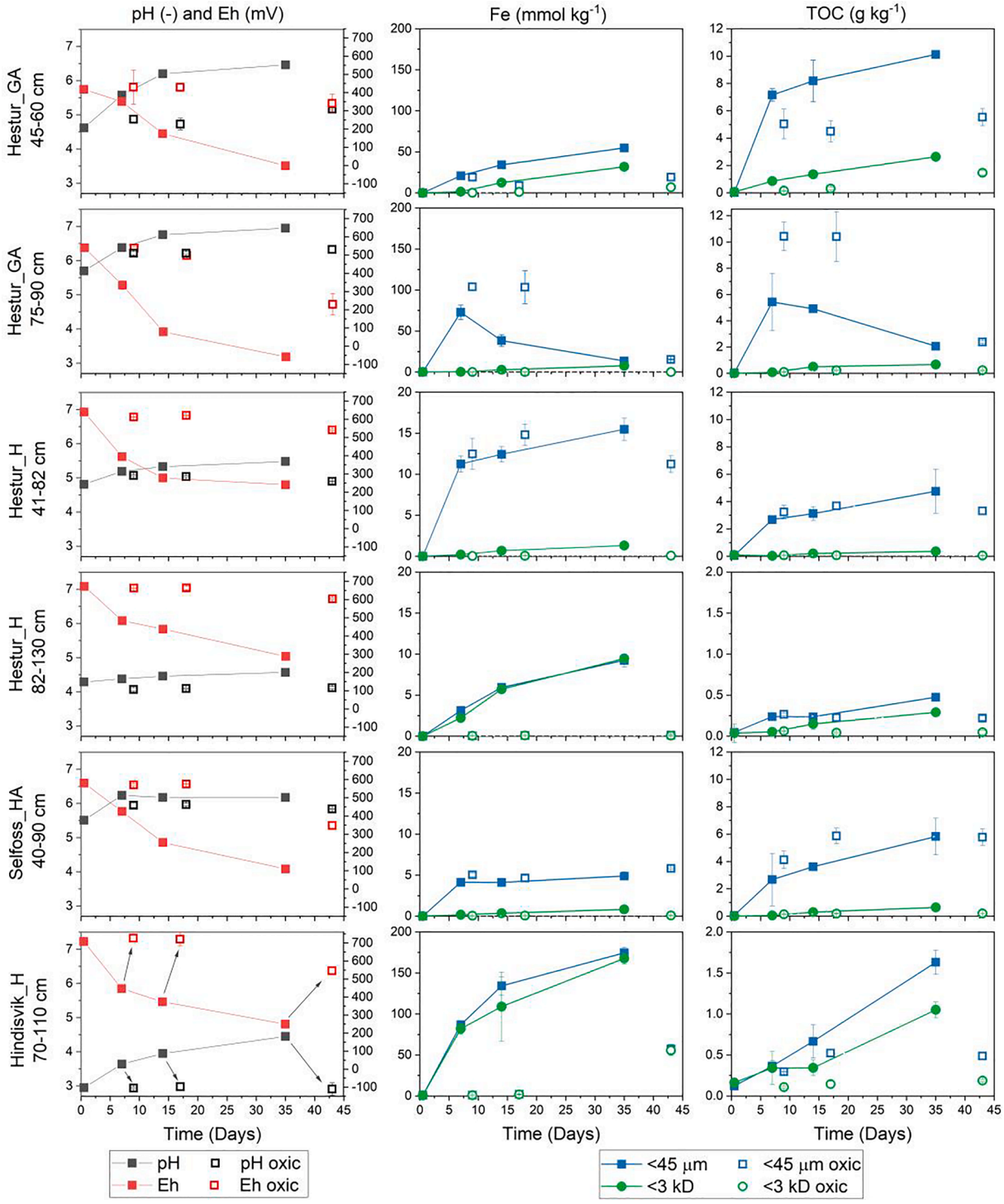

Fig. 1. Trends during anoxic/oxic soil incubation (1:10 soil:water ratio) in pH, Eh (left panel) and aqueous Fe (middle panel) and OC (right panel) determined in <0.45 µm and <3 kDa filtrates, shown in blue and green, respectively. Error bars indicate the standard deviation calculated from triplicate experiments. Closed symbols show sampling conducted under anoxic conditions while subsequent open symbols show corresponding sampling after soil slurry re-oxidation. To help explain this visually, demonstrative arrows are included in the lower left panel, indicating related anoxic and oxic sampling points. (For interpretation of the references to colour in this figure legend, the reader is referred to the web version of this article.)

fraction were highest in Hestur_GA_45-60 (10.1 g kg^{-1}), while the lowest amounts were determined for Hestur_H_82-130 and Hindisvik_H_70-100 (0.48 and 1.63 g kg^{-1}, respectively). Moreover, while at start of the incubation, total OC desorbed from the soils was similar in both the <0.45-µm and <3 kDa fractions of all soils (<0.12 g kg^{-1} (x^{-} = 0.06) and <0.16 g kg^{-1} (x^{-} = 0.06), respectively), after 5 weeks of anoxic incubation, higher amounts of OC were generally found in the <0.45-µm fraction, suggesting that OC was mobilized concomitantly with the colloidal fraction.

3.3. Trends in aqueous geochemistry after soil slurry re-oxidation

Following 1 and 2 weeks of anoxic incubation, all soil slurries rapidly re-oxidized upon exposure to ambient air (for 2 or 4 days, respectively),

reaching similar Eh and pH conditions as recorded at the start of the incubation (Fig. 1, left panel, open symbols). After 5 weeks of anoxic incubation, 8 days of exposure to ambient air returned the soil slurry pH values similar to those at the experiment start, however redox potential remained slightly lower than at the start of the experiment (Fig. 1, left panel, open symbols). For Fe, OC, and other elements mobilized as colloids under anoxic conditions, similar element concentrations were determined in the colloidal fraction after reoxidation (Fig. 1, middle and right panels, Figures S7-S9, all panels, open symbols). In contrast, for the re-oxidized Hestur_H_82-130 and Hindisvik_H_70-100, soil horizons which did not mobilize Fe in colloids under anoxic conditions, amounts of aqueous Fe in both <0.45-μm and <3 kDa fractions were near zero, suggesting that oxidation of the aqueous Fe(II) in these samples resulted in the removal of Fe from solution. However, amounts of aqueous OC, Al, Mn, Si, Ca, Mg, N, and S appeared less affected by soil slurry re-oxidation in Hestur_H_82-130 and Hindisvik_H_70-100; aqueous OC concentrations in both the <0.45-μm and <3 kDa fractions of the re-oxidized slurries were only slightly lower than under anoxic conditions, while the other elements (Al, Mn, Si, Ca, Mg, N, and S) persisted primarily in the <3 kDa fraction in amounts similar to those measured under anoxic conditions.

3.4. Solid-phase iron speciation: Chemical extractions

Changes in solid-phase chemical forms of Fe prior to and during incubation and subsequent re-oxidation were qualitatively assessed with parallel selective chemical extractions, presented in Table 3. For most soil horizons, anoxic incubation resulted in changes in the fractions of ammonium oxalate (O) and sodium pyrophosphate (P) extractable Fe. Decreases in Fe_O were recorded for Hestur_GA_75-90, Hestur_H_41-82, and Hindisvik_H_70-110 at all timepoints (up to –22, –32, and −37 %, in each soil horizon, respectively). However, decreases in Fe_O only occurred after 5 weeks of anoxic incubation for Hestur_H_82-130 and Selfoss_HA_40-90 (-20 and −7%, respectively). In contrast, increases in Fe_O were reported for Hestur_GA_45-60 at each timepoint (up to +12 %). Re-oxidation of the soil slurries resulted in overall higher amounts of Fe_O in the Hestur_GA horizons, while in other soil horizons Fe_O remained similar (Hestur_H horizons, Selfoss_HA_40-90) or even decreased (Hindisvik_H_70-110) compared to initial amounts of Fe_O. Changes in Fe_P during anoxic incubation were more similar amongst all the soil horizons, with increases recorded for most soils. Re-oxidation of the soil slurries resulted in slightly lower amounts of Fe_P compared to under anoxic conditions at each timepoint, but overall amounts of Fe_P were higher than initial values. An exception is noted for the soil horizons Hestur_H_41-82 and Hindisvik_H_70-110, where amounts Fe_P decreased both under anoxic incubation and additionally following re-oxidation.

3.5. Solid-phase iron speciation: Fe K-edge XAS

Iron oxidation state and speciation in the soil horizons and changes in Fe speciation following 5 weeks of anoxic incubation and subsequent re-oxidation were assessed with Fe *K*-edge XAS. Initially, normalized Fe *K*-edge XANES spectra of the soil samples exhibited a first-derivative maxima at ~7128 eV, implying the predominance of Fe(III) (Figure S10A). Unreacted Selfoss_HA_40-90 is an exception, as the normalized first derivative of the XANES spectra shows features similar to an Fe(II)-containing silicate (e.g., the chemically-reduced smectite (SWa-1_red)). Bulk soil Fe speciation, determined through LCF analyses of Fe *K*-edge EXAFS spectra, is reported in Table 4 and spectra and model fits are shown in Fig. 2. Iron speciation in soil horizons from the same site (e.g., Hestur_GA_45-60 and _75-90 and Hestur_H_41-82 and _82-130) were most similar to each other. Iron in the Hestur_GA soil horizons comprised 32–42 % ferrihydrite. These numbers are in relatively good agreement with the high fraction of soil Fe in poorly-crystalline mineral phases extracted by acid ammonium oxalate (Fe_O = 50–61 % of Fe_T, Table 2 and Table S1). Goethite accounted for 8–11 % of soil Fe in the Hestur_GA soil horizons. In contrast, Fe in the Hestur_H soil horizons was dominated by goethite (51–66 % of total Fe) whereas ferrihydrite

Table 3
Results from selective chemical extractions of the initial, reduced, and re-oxidized soils.

Soil sample	Redox cycle duration	Fe_O[a]			Fe_P[b]		
		initial	anoxic	oxic	initial	anoxic	oxic
	(anoxic/oxic days)	(mg g^{-1})	(mg g^{-1})	(mg g^{-1})	(mg g^{-1})	(mg g^{-1})	(mg g^{-1})
Hestur_GA _45-60	initial	31.67			22.77		
	7/2		31.28	38.46		35.58	32.90
	14/4		34.02	38.31		37.21	32.43
	35/8		35.42	38.14		46.65	36.21
Hestur_GA _75-90	initial	74.30			9.69		
	7/2		68.11	96.37		21.05	13.16
	14/4		67.17	87.43		24.42	14.20
	35/8		58.19	93.02		25.01	18.13
Hestur_H _41-82	initial	14.22			35.48		
	7/2		11.94	12.32		28.91	28.56
	14/4		10.52	9.91		31.13	24.38
	35/8		9.65	12.52		30.34	29.88
Hestur_H _82-130	initial	10.96			9.46		
	7/2		12.65	10.77		21.33	21.54
	14/4		11.54	11.71		24.68	21.71
	35/8		8.75	NM		21.97	NM
Selfoss_HA _40-90	initial	8.36			4.88		
	7/2		8.78	7.25		6.98	5.89
	14/4		8.53	6.79		7.12	5.22
	35/8		7.78	8.59		8.07	6.49
Hindisvik_H_70-110	initial	80.03			53.11		
	7/2		52.24	40.04		41.91	35.56
	14/4		63.48	40.10		49.52	26.72
	35/8		49.90	62.67		44.28	37.26

[a] Acid ammonium oxalate extraction (Loeppert and Inskeep, 1996).
[b] Sodium-pyrophosphate treatment (McKeague, 1967). NM = samples were not measured due to limited material available. Additional results from selective chemical extractions for Al and Si are found in Table S2.

Table 4
Linear combination fit results for Fe *K*-edge EXAFS spectra of initial and 5 week anoxic incubated (_Red) and re-oxidized (_Ox) soils.

Soil sample	Fh	Gt	Lp	Fe(III)-clay	Fe(II)-clay	Fe(III)-organic	Fe(II)-organic	NSSR[a]	red. χ^2[b]
	(%)	(%)	(%)	(%)	(%)	(%)	(%)	(%)	(-)
Hestur_GA_45-60	32	12		49		8		1.11	0.074
Hestur_GA_45-60_Red		6		73		11	11	1.37	0.072
Hestur_GA_45-60_Ox	35	5		43		18		1.03	0.026
Hestur_GA_75-90	42	8		50				1.97	0.095
Hestur_GA_75-90_Red	26	12		48	14			2.80	0.113
Hestur_GA_75-90_Ox	45	11		44				1.49	0.079
Hestur_H_41-82		66		20		14		4.05	0.242
Hestur_H_41-82_Red		72		10		18		4.64	0.329
Hestur_H_41-82_Ox		68		12		21		4.29	0.287
Hestur_H_82-130		51		26		22		2.85	0.182
Hestur_H_82-130_Red		72		11		17		4.31	0.287
Hestur_H_82-130_Ox		68		13		19		4.17	0.270
Selfoss_HA_40-90	33		12		23	32		6.53	0.155
Selfoss_HA_40-90_Red	12			49		38		7.28	0.271
Selfoss_HA_40-90_Ox	34			33		33		2.84	0.16
Hindisvik_H_70-110	33			31		36		5.04	0.355
Hindisvik_H_70-110_Red				43		34	23	5.17	0.212
Hindisvik_H_70-110_Ox	26	17		20		36		2.53	0.162

[a] NSSR: Normalized sum of squared residuals ($100\times\sum_i(data_i\text{-}fit_i)^2/\sum_i data^2$).
[b] Fit accuracy (reduced $\chi^2 = (N_{idp}/N_{pts})\sum_i((data_i\text{-}fit_i)/\varepsilon_i)^2(N_{idp}\text{-}N_{var})^{-1}$. N_{idp}, N_{pts} and N_{var} are, respectively, the number of independent points in the model fit (21), the total number of data points (201), and the number of fit variables (3–4). ε_i is the uncertainty of the i^{th} data point.(Kelly et al., 2008) Abbreviations: Fh = ferrihydrite, Gt = goethite, Lp = lepidocrocite, Fe(III)-clay = fit as a combination of 1Mt-1 (illite; 5 wt% Fe) and/or SWa-1 (ferruginous smectite; 18 wt% Fe). Fe(II)-clay = fit as SWa-1_red. Fe(III)-organic = fit as Fe(III)-citrate or Fe(III)-oxalate, Fe(II)-organic = Fe(II)-gluconate.

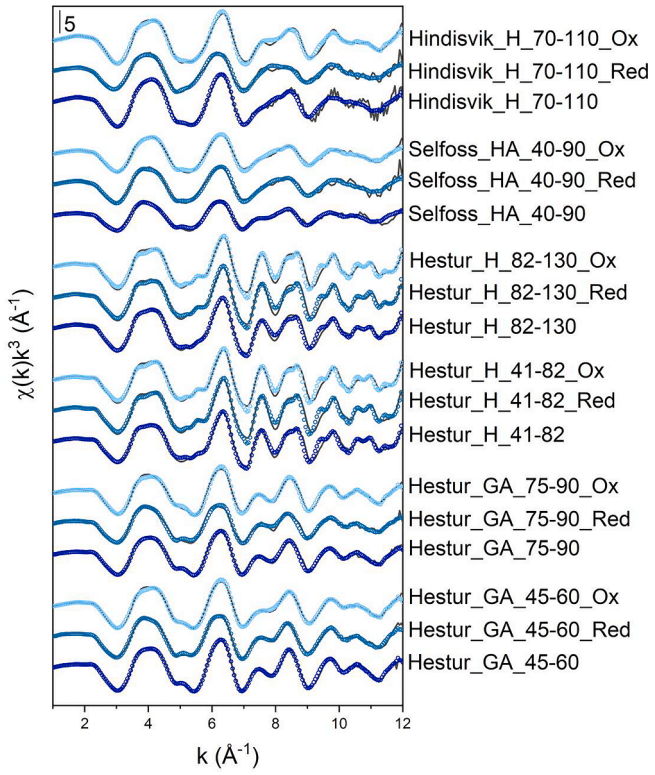

Fig. 2. Iron *K*-edge EXAFS spectra of initial, 5-week anoxic incubated (_Red) and re-oxidized (_Ox) soils and their linear combination fits (LCF). Experimental data is shown as solid lines and model fits are shown as symbols. Fit results are reported in Table 3, reference spectra are shown in Figure S12.

was not detected (<5 mol %), in agreement with lower fractions of acid ammonium oxalate extractable Fe (Fe_O = 17–40 % of Fe_T, Table 2 and Table S1). Both Selfoss_HA_40-90 and Hindisvik_H_70-110 also contained Fe in ferrihydrite (both 33 % of total Fe), however goethite was not found in either of these soil horizons. All soil horizons also contained Fe in clay minerals (20–57 % of total Fe), which was fit as a combination of multiple Fe-containing reference spectra (1Mt-1, illite, 5 wt% Fe; SWa-1, ferruginous smectite, 18 wt% Fe, or SWa-1_red). Additionally, Fe (III)-organic complexes, modeled with reference spectra for Fe(III)-citrate and Fe(III)-oxalate, contributed to 14–36 % of total Fe in the Hestur_H soil horizons, Selfoss_HA_40-90, and Hindisvik_H_70-110.

Following 5 weeks of anoxic incubation, the appearance of a shoulder at or a shift in the first-derivative maxima of Fe *K*-edge XANES spectra to ~ 7125 eV indicated the formation of solid-associated Fe(II) (Figure S10A). Changes in the Fe oxidation state of the reduced soil horizons were quantified by LCF analyses of Fe *K*-edge XANES spectra, reported in Table S5 and shown in Figure S10B. In agreement with trends in aqueous Fe (Fig. 1, middle panel), the fraction of solid-associated Fe(II) increased (+23 % to +33 % of total Fe) in reduced soil horizons which produced the highest maximum amounts aqueous Fe during the 5-week incubation (>50 mmol kg^{-1}, Hestur_GA_45-60 and _75-90 and Hindisvik_H_70-110). In contrast, the solid-associated Fe(II) fraction in the Hestur_H horizons (_41-82 and _82-130) remained similar (±4%), while the solid-associated Fe(II) fraction decreased in both Hestur_H_41-82 (-4%) and Selfoss_HA_40-90 (-18 %), in agreement with the relatively low aqueous Fe measured in these samples over the 5-week incubation (<16 mmol kg^{-1}).

Solid-phase Fe speciation after 5 weeks of anoxic incubation revealed changes in soil Fe mineral composition. For soil horizons initially containing ferrihydrite or lepidocrocite, contributions from these minerals were noticeably absent or significantly reduced after anoxic incubation (Fig. 2, Table 4). The reductive dissolution of ferrihydrite or lepidocrocite resulted in a relative increase in the fraction of Fe found in clay minerals and/or organically-complexed Fe(III), but did not appear to contribute to the formation of crystalline Fe mineral phases like goethite. In contrast, for Hestur_H horizons, the relative fraction of Fe found in goethite increased under reducing conditions seemingly at the expense of Fe in clay minerals. Organically-complexed Fe(II), modeled with reference spectra for Fe(II)-gluconate, was found in the anoxic incubated Hestur_GA_45-60 and Hinsidvik_H_70-110 soil horizons.

Following re-oxidation, the first-derivative maxima of Fe *K*-edge XANES spectra returned to ~7128 eV (Figure S10A), suggesting again the dominance of Fe(III) in the soils similar to the Fe oxidation state pre-reduction. Indeed, LCF analyses of the re-oxidized soil samples indicated that Fe(III) accounted for similar (Hestur_GA_45-60, Hestur_H_82-130, Hindisvik_H_70-110) or even higher (Hestur_GA_75-90, Hestur_H_41-

82, Selfoss_HA_40-90) fractions than pre-reduction. Iron mineral speciation in the re-oxidized soil samples was similar to that of the initial soils (Table 4). Specifically, overall ferrihydrite fractions in the re-oxidized soils accounted for 26–45 % of total solid-phase Fe, compared to 28–39 % pre-reduction. For the Hestur_GA horizons, slight increases in the overall ferrihydrite fractions (+3%) are in agreement with overall increases in the amount of Fe_O (Table 3), while for Hindisvik_H_70-110, the lower ferrihydrite contribution (-7%) in favor of new goethite (+17 %) in the re-oxidized soil samples may explain the decrease in Fe_O (Table 3). In the Hestur_H horizons, where no ferrihydrite was initially present, Fe mineral speciation was dominated by goethite and Fe(III) in clay, again mirroring pre-reduction Fe mineral speciation. Fractions of organically-complexed Fe(II) formed during anoxic incubation were likely recovered as organically complexed Fe(III) upon re-oxidation.

4. Discussion

4.1. Microbial reduction of Fe(III)

Flooding of the soil horizons and the onset of anoxia resulted in a drop in redox potential in the first 1 to 2 weeks, after which time further decreases in the redox potential were noticeably less. After 5 weeks of anoxic incubation, the measured redox potentials of the soil horizons studied here were significantly higher than those measured during anoxic incubation of other organic-rich (22–33 wt% C) volcanic soils over shorter (3 weeks) incubation periods (compare $Eh_7 = 152$ to -60 mV in the soil horizons studied here (Figure S6) to $Eh_7 = -254$ to -319 mV in Buettner, et al. (Buettner et al., 2014)). The maintenance of higher redox potentials likely results from the high amounts of easily reducible Fe in the soils (Fe_O, Table S1), which may have poised the redox potential at the Fe^{3+}/Fe^{2+} redox couple, thus promoting Fe(III) as a terminal electron acceptor. Microbial reduction of Fe(III) to Fe(II) in our soil microcosms agrees well with the findings of Opfergelt et al., (Opfergelt et al., 2017) who measured variations in Fe isotope compositions *in-situ* in bulk soil and soil solution sampled in poorly drained peat soils of Iceland. Their measurements showed that the Fe isotope composition of the soil solutions was lighter than the bulk soil ($\Delta^{57}Fe_{solution\text{-}soil} = 0.41 \pm 0.32$ ‰), indicating the mobilization of Fe in peat porewater by reductive mineral dissolution and/or ligand-controlled dissolution.

In soils, microbial reduction of Fe(III) is coupled to the oxidation of OC (Melton et al., 2014). Therefore, while all soil horizons were rich in organic material (21 to 43 wt% C), among the soil horizons selected for this study, a primary variable was the range of C:Fe molar ratios, which spanned 8.1 to 74. The results showed, however, that the extent of Fe (III) reduction did not correlate to these molar ratios (compare Table 2 and Table S5). Instead, the fraction of total Fe extractable in acid ammonium oxalate extraction offered insights, whereby low Fe_O/Fe_D ratios corresponded to lower solid-associated Fe(II) under anoxic conditions and soil horizons with the highest Fe_O/Fe_D ratios underwent the most Fe(III) reduction (compare Tables S1 and S8).

4.2. Mobilization and elemental composition of colloids

Under anoxic conditions, the reductive dissolution of Fe minerals led to the release of colloids in some, but not all, of the organic soil horizons included here. The mechanisms governing colloid mobilization through changes in surface charge are well studied and are influenced by changes in geochemical parameters of the soil solution (e.g., pH, Eh, solution chemistry, or ionic strength) (Ryan and Gschwend, 1994). Specifically, as pH increases above the point of zero charge (p.z.c.) of the colloid, interparticle electrostatic repulsion results in the dispersion of the colloids (Buettner et al., 2014). Considering the high organic content of the soil horizons studied here (Table 2), it seems plausible that the soils have a low p.z.c. (pH <4), making pH-promoted colloid dispersion likely. However, pH changes alone may not account for colloid mobilization. For example, far more colloids are released when pH changes are accompanied by or attributed to Fe reduction (Buettner et al., 2014). The consumption of protons during the reductive dissolution of Fe(III) minerals leads to an increase in pH (Vepraskas et al., 2016), but the reduction of Fe(III) minerals may additionally promote colloid dispersion by dissolving the SRO-mineral phases acting as connective cement holding soil aggregates together (Ryan and Gschwend, 1992). All soil horizons studied here showed evidence of Fe(III) reduction, seen as increases in aqueous (Fig. 1, middle panel) or solid-associated Fe(II) (Table S5) during anoxic incubation, and increases in pH were similarly recorded in all soil horizons (Fig. 1, left panel). Yet little to no colloid mobilization occurred for Hestur_H_82-130 and Hindisvik_70-110. That these soils reached pH ~ 4.5 after 5 weeks of anoxic incubation (Fig. 1, left panel) and no colloids were mobilized indicates that either (1) soil aggregates were very stable or that (2) the p.z.c. of colloids in these soil horizons is at least pH 4.5. The p.z.c. expected for mineral colloids with organic matter coatings is pH <4 (Chorover and Sposito, 1995). A slightly higher p.z.c in the soil horizons studied here may suggest a significant organic-poor mineral component, potentially consisting of organic-poor ferrihydrite (p.z.c. pH 5–8) (ThomasArrigo et al., 2019) or aluminosilicates (e.g., allophane or imogolite, p.z.c. pH >6) (Su and Harsh, 1996).

Mobilized colloids persisted during re-oxidation in all other soil horizons. This may similarly be explained by pH, whereby, despite decreases during oxidation (Fig. 1, left panel), pH values remained above or near 4.6. At all timepoints (oxic and anoxic), the colloids primarily comprised OC, with an average Fe:Al:OC molar ratio of 2.7:1:54 (Table S4). The Fe and Al content of the colloids in this study is much higher compared to colloids collected in porewaters of peat soils across a permafrost thaw gradient (Fe:Al:OC = 1.9:1:308) (Raudina et al., 2021), and likely reflects the high mineral content of the Iceland soils. While slightly higher Fe:Al molar ratios were found in colloids under anoxic conditions compared to re-oxidized colloids ($\bar{x} = 3.2$ vs 2.1, Table S4), the elemental ratios in the colloids were generally consistent, suggesting that colloid chemical composition was not impacted by the changing redox conditions, as has been similarly reported for colloids mobilized during recursive redox cycles in tropical volcanic soils (Thompson et al., 2006a).

In the absence of colloid mobilization under anoxic conditions, oxidation of the Hestur_H_82-130 and Hindisvik_70-110 soil slurries resulted in the removal of all aqueous Fe and most aqueous OC in Hestur_H_82-130 and Hindisvik_70-110. Aqueous Fe was found to comprise primarily Fe(II) and thus could have existed as both freely dissolved Fe(II) or in Fe(II)-organic complexes. Therefore, the removal of Fe and OC from solution upon oxidation suggests the adsorption and/or coprecipitation of the aqueous OC or Fe(II/III)-organic complexes with residual or newly-formed Fe(III) minerals (Bhattacharyya et al., 2018) or the existing soil matrix or Fe(III)-promoted aggregation.

4.3. Contrasting shifts in iron mineral transformations during redox cycles

The trajectory of Fe mineral transformations during redox cycles in natural soils is not clear, with both increases (Mejia et al., 2016; Thompson et al., 2006b; Ye et al., 2019) and decreases (Coby et al., 2011; Thompson et al., 2011; Vogelsang et al., 2016; Winkler et al., 2018; Ye et al., 2019) in soil SRO-fractions reported. Factors such as starting mineral phase crystallinity (Coby et al., 2011; Thompson et al., 2006b; Winkler et al., 2018) and pO_2 (Chen and Thompson, 2018; Chen et al., 2018; Wilmoth et al., 2018) may be important, and model studies have shown that both the reductive dissolution and transformation of Fe minerals under anoxic conditions (Hansel et al., 2005; ThomasArrigo et al., 2020; ThomasArrigo et al., 2018; ThomasArrigo et al., 2019; ThomasArrigo et al., 2017; Zhou et al., 2018) and the products of oxidation of dissolved Fe(II) (Chen and Thompson, 2018; Daugherty et al., 2017; Kinsela et al., 2016; Senn et al., 2015) are strongly impacted

by porewater geochemistry, including the presence of OM (Chen and Thompson, 2018; Daugherty et al., 2017; ThomasArrigo et al., 2020; ThomasArrigo et al., 2018; ThomasArrigo et al., 2019; ThomasArrigo et al., 2017; Zhou et al., 2018). Under anoxic conditions, SRO Fe minerals are prone to rapid reductive dissolution compared to crystalline mineral phases (Roden and Zachara, 1996). This likely explains the absence or strong decrease in ferrihydrite fractions in the reduced soil horizons and suggests that the lepidocrocite initially present in Selfoss_HA_40-90 was also poorly crystalline. However, microbially-derived Fe(II) may also drive Fe(II)-catalyzed transformation of SRO Fe minerals towards more thermodynamically stable mineral phases in anoxic soils (e.g., lepidocrocite, goethite, or magnetite) (Giannetta et al., 2020). In our study, the absence of significant increases in crystalline mineral phases under reducing conditions may result from the abundance of OM or the slightly acidic pH conditions, both factors which inhibit Fe(II)-catalyzed mineral transformation (ThomasArrigo et al., 2018; ThomasArrigo et al., 2019; ThomasArrigo et al., 2017). Alternatively, dissolved Fe(II) may have otherwise interacted with the soil matrix; forming Fe(II)-organic complexes (e.g., in Hestur_GA_45-60 and Hindisvik_H_70-110, Table 4), or participated in electron transfer and Fe atom exchange with existing clay minerals (Van Groeningen et al., 2020).

Upon re-oxidation, the resurgence of ferrihydrite fractions in the soils suggests the rapid oxidation of solid-associated or aqueous Fe(II); a process which is likely to widely occur *in-situ*: As the majority of wetlands in Iceland are minerotrophic (Arnalds et al., 2016), the continual influx of Fe-rich anoxic porewater combined with the oxidation of Fe(II) in surface soil horizons caused by water table fluctuations or wetland drainage may account for the high accumulation of Fe in the soil horizons. Indeed, recent modeling of the thermodynamic stability of Fe phases in Icelandic peat soils suggests that ferrihydrite is expected to be dominant (Linke and Gislason, 2018). However, neoformation of ferrihydrite occurred only in soil horizons which initially contained ferrihydrite. In contrast, in the Hestur_H soil horizons, which comprised only goethite, Fe(III) in clays, and organically-complexed Fe(III) at all times during the incubation, ferrihydrite did not form above detection limits for LCF of Fe *K*-edge EXAFS spectra (>5 % of total Fe), yet the relative goethite fraction increased again slightly during oxidation. These results may suggest that the oxidizing Fe(II) preferentially formed goethite (rather than ferrihydrite) in the presence of existing goethite. However, the high content of goethite and lack of ferrihydrite in the initial soil Fe mineral composition likely led to overall reduced reductive dissolution. This is demonstrated in the minimal change in solid-associated Fe(II) and lower concentrations of aqueous Fe seen under anoxic conditions, and also implies that little Fe(II) was available to oxidize. Therefore, we cannot assess preferential precipitation of crystalline versus poorly crystalline mineral phases during re-oxidation. Yet, the general similarities in Fe mineral contributions seen between the initial and the re-oxidized soil horizons suggest that initial soil mineral crystallinity influences the trajectory of Fe mineral transformations during redox cycling, in agreement with literature (Coby et al., 2011; Thompson et al., 2006b; Winkler et al., 2018).

5. Conclusions

In this soil incubation study, Fe-rich, organic soils from Iceland were exposed to redox cycles comprising of 1, 2 or 5 weeks of anoxic incubation followed by re-oxidation. Initial soil Fe mineral composition influenced the trajectory of Fe mineral transformations. Specifically, soil horizons containing SRO Fe mineral phases (ferrihydrite and lepidocrocite) underwent more extensive Fe reduction, simultaneously facilitating more Fe(II) oxidation and new ferrihydrite formation upon re-oxidation. In contrast, Fe reduction in soil horizons comprising initially more crystalline Fe mineral phases (e.g., goethite) was limited and the mineral phases were generally preserved during redox cycles.

For most soil horizons, changes in porewater geochemistry, specifically increases in pH caused by microbial reduction of SRO Fe mineral phases under anoxic conditions, promoted the mobilization of SOC as organic-Fe-/Al-colloids which remained in suspension even after re-oxidation. Moreover, mobilization of the colloidal fraction occurred as early as 1 week after anoxic incubation. These results suggest that increases in the frequency of redox cycles, potentially caused by changes in hydrologic regimes associated to climate change, may lead to an increased mobilization of SOC as organic-Fe-/Al-colloids. At the same time, in soil horizons that exhibited overall lower pH, aqueous phase Fe and OC was removed from solution after re-oxidation. As increases in pH are related to the reductive dissolution of Fe(III) minerals, shorter redox cycles which limit the extent of microbial reduction of Fe(III) may decrease the amount of aqueous Fe and OC released in low pH soils. For Icelandic wetlands, mobilization of colloids and aqueous Fe and OC has further implications for the export of Fe and C from wetlands to coastal waters: currently an estimated 30,000 km of ditches drain Icelandic wetland soils, affecting nearly 47 % of all Icelandic wetlands and 70 % of wetlands situated below 200 m elevation (Arnalds et al., 2016). Considering the proximity of these low elevation wetlands and drainage networks to the coast, it is plausible that mobilized colloids may contribute to increases in particulate suspended matter released to coastal waters with increased redox cycling.

Declaration of Competing Interest

The authors declare that they have no known competing financial interests or personal relationships that could have appeared to influence the work reported in this paper.

Data availability

Data will be made available on request.

Acknowledgments

We are grateful to K. Barmettler and S. Heller (ETH Zurich) for assisting with laboratory analyses. We thank A. Thompson (University of Georgia), Ó. Arnalds and H. Óskarsson (Agricultural University of Iceland; AUI) for their helpful discussions and the AUI for providing accommodation during field campaigns. We also thank the Icelandic Meteorological Office (IMO) for providing temperature and precipitation data (Icelandic Meteorological Office (IMO) 2022: Icelandic Meteorological Office Database, delivery no. 2022-02-08/GEJ01 and 2022-02-08/GEJ01b). We acknowledge SOLEIL (Proposals no. 20200766 and no. 20190784) and Elettra (Proposal no. 20215105) for the provision of synchrotron radiation facilities and thank D. Vantelon (LUCIA beamline), G. Landrot (SAMBA beamline), D. Oliviera de Souza (XAFS beamline) for their support during the synchrotron measurements. This work was funded by the Swiss Polar Institute Polar Access Fund (L. ThomasArrigo; PAF-2020-03), an ETH Career Seed Grant (L. ThomasArrigo; SEED-13 18-2) and received funding from the European Research Council (ERC) under the European Union's Horizon 2020 research and innovation programme (R. Kretzschmar; Grant agreement No. 788009-IRMIDYN-ERC-2017-ADG).

Appendix A. Supplementary data

Supplementary data to this article can be found online at https://doi.org/10.1016/j.geoderma.2022.116217.

References

Arnalds, O., 2004. Volcanic soils of Iceland. Catena 56 (1-3), 3–20.
Arnalds, O., 2010. Dust sources and deposition of aeolian materials in Iceland. Iceland. Agr. Sci. 23, 3–21.
Arnalds, O., 2015. The Soils of Iceland. Springer Science+Business Media.

Arnalds, O., Gudmundsson, J., Oskarsson, H., Brink, S.H., Gisladottir, F.O., 2016. Icelandic inland wetlands: Characteristics and extent of draining. Wetlands 36 (4), 759–769.
Baker, L.L., Nickerson, R.D., Strawn, D.G., 2014. XAFS study of Fe-substituted allophane and imogolite. Clay. Clay Miner. 62 (1), 20–34.
Barcellos, D., Cyle, K.T., Thompson, A., 2018. Faster redox fluctuations can lead to higher iron reduction rates in humid forest soils. Biogeochemistry 137 (3), 367–378.
Bekryaev, R.V., Polyakov, I.V., Alexeev, V.A., 2010. Role of polar amplification in long-term surface air temperature variations and modern Arctic warming. J. Climate 23, 3888–3906.
Bhattacharyya, A., Campbell, A.N., Tfaily, M.M., Lin, Y., Kukkadapu, R.K., Silver, W.L., Nico, P.S., Pett-Ridge, J., 2018. Redox fluctuations control the coupled cycling of iron and carbon in tropical forest soils. Environ. Sci. Technol. 52 (24), 14129–14139.
Bonatotzky, T., Ottner, F., Erlendsson, E., Gísladóttir, G., 2019. The weathering of volcanic tephra and how they impact histosol development. An example from South East Iceland. Catena 172, 634–646.
Bonatotzky, T., Ottner, F., Erlendsson, E., Gísladóttir, G., 2021. Weathering of tephra and the formation of pedogenic minerals in young Andosols, South East Iceland. Catena 198, 105030.
Buettner, S.W., Kramer, M.G., Chadwick, O.A., Thompson, A., 2014. Mobilization of colloidal carbon during iron reduction in basaltic soils. Geoderma 221, 139–145.
Chen, C., Thompson, A., 2018. Ferrous iron oxidation under varying pO_2 levels: The effect of Fe(III)/Al(III) oxide minerals and organic matter. Environ. Sci. Technol. 52 (2), 597–606.
Chen, C., Meile, C., Wilmoth, J., Barcellos, D., Thompson, A., 2018. Influence of pO_2 on iron redox cycling and anaerobic organic carbon mineralization in a humid tropical forest soil. Environ. Sci. Technol. 52 (14), 7709–7719.
Chorover, J., Sposito, G., 1995. Colloid chemistry of kaolinitic tropical soils. Soil Sci. Soc. Am. J. 59, 1558–1564.
Coby, A.J., Picardal, F., Shelobolina, E., Xu, H.F., Roden, E.E., 2011. Repeated anaerobic microbial redox cycling of iron. Appl. Environ. Microb. 77, 6036–6042.
Coward, E.K., Thompson, A.T., Plante, A.F., 2017. Iron-mediated mineralogical control of organic matter accumulation in tropical soils. Geoderma 306, 206–216.
Coward, E.K., Thompson, A., Plante, A.F., 2018. Contrasting Fe speciation in two humid forest soils: Insight into organomineral associations in redox-active environments. Geochim. Cosmochim. Acta 238, 68–84.
Dahlgren, R.A., 1994. Quantification of Allophane and Imogolite. In: Amonette, J.E., Zelanzy, L.W. (Eds.), Quantitative Methods in Soil Mineralogy. Soil Science Society of America, Madison, WI, USA, pp. 430–451.
Daugherty, E.E., Gilbert, B., Nico, P.S., Borch, T., 2017. Complexation and redox buffering of iron(II) by dissolved organic matter. Environ. Sci. Technol. 51 (19), 11096–11104.
Dubinsky, E.A., Silver, W.L., Firestone, M.K., 2010. Tropical forest soil microbial communities couple iron and carbon biogeochemistry. Ecology 91 (9), 2604–2612.
Eswaran, H., Vandenberg, E., Reich, P., 1993. Organic carbon in soils of the world. Soil Sci. Soc. Am. J. 57, 192–194.
Fadrus, H., Malý, J., 1975. Supression of iron(III) interference in determination of iron (II) in water by 1,10-phenanthroline method. Analyst 100, 549–554.
Filimonova, S., Kaufhold, S., Wagner, F.E., Häusler, W., Kögel-Knabner, I., 2016. The role of allophane nano-structure and Fe oxide speciation for hosting soil organic matter in an allophanic Andosol. Geochim. Cosmochim. Acta 180, 284–302.
Georg, R.B., Reynolds, B.C., West, A.J., Burton, K.W., Halliday, A.N., 2007. Silicon isotope variations accompanying basalt weathering in Iceland. Earth Planet. Sc. Lett. 261, 476–490.
Giannetta, B., Balint, R., Said-Pullicino, D., Plaza, C., Martin, M., Zaccone, C., 2020. Fe (II)-catalyzed transformation of Fe (oxyhydr)oxides across organic matter fractions in organically amended soils. Sci. Total Environ. 748, 141125.
Ginn, B., Meile, C., Wilmoth, J., Tang, Y., Thompson, A., 2017. Rapid iron reduction rates are stimulated by high-amplitude redox fluctuations in a tropical forest soil. Environ. Sci. Technol. 51 (6), 3250–3259.
Gu, B., Schmitt, J., Chen, Z., Liang, L., McCarthy, J.F., 1994. Adsorption and desorption of natural organic matter on iron oxide: Mechanisms and models. Environ. Sci. Technol. 28 (1), 38–46.
Hall, S.J., Silver, W.L., 2013. Iron oxidation stimulates organic matter decomposition in humid tropical forest soils. Glob. Change Biol. 19 (9), 2804–2813.
Handler, R.M., Frierdich, A.J., Johnson, C.M., Rosso, K.M., Beard, B.L., Wang, C., Latta, D.E., Neumann, A., Pasakarnis, T., Premaratne, W.A.P.J., Scherer, M.M., 2014. Fe(II)-catalyzed recrystallization of goethite revisited. Environ. Sci. Technol. 48 (19), 11302–11311.
Hansel, C.M., Benner, S.G., Fendorf, S., 2005. Competing Fe(II)-induced mineralization pathways of ferrihydrite. Environ. Sci. Technol. 39 (18), 7147–7153.
Harðarson, B.S., Fitton, J.G., Hjartarson, A., 2008. Tertiary volcanism in Iceland. Jokull 58, 161–178.
Hawley, S.M., von Strandmann, P., Burton, K.W., Williams, H.M., Gíslason, S.R., 2017. Continental weathering and terrestrial (oxyhydr)oxide export: Comparing glacial and non-glacial catchments in Iceland. Chem. Geol. 462, 55–66.
Hindshaw, R.S., Bourdon, B., Pogge von Strandmann, P.A.E., Vigier, N., Burton, K.W., 2013. The stable calcium isotopic composition of rivers draining basaltic catchments in Iceland. Earth Planet. Sc. Lett. 374, 173–184.
Hinzman, L.D., Bettez, N.D., Bolton, W.R., Chapin, F.S., Dyurgerov, M.B., Fastie, C.L., Griffith, B., Hollister, R.D., Hope, A., Huntington, H.P., Jensen, A.M., Jia, G.J., Jorgenson, T., Kane, D.L., Klein, D.R., Kofinas, G., Lynch, A.H., Lloyd, A.H., McGuire, A.D., Nelson, F.E., Oechel, W.C., Osterkamp, T.E., Racine, C.H., Romanovsky, V.E., Stone, R.S., Stow, D.A., Sturm, M., Tweedie, C.E., Vourlitis, G.L., Walker, M.D., Walker, D.A., Webber, P.J., Welker, J.M., Winker, K.S., Yoshikawa, K., 2005. Evidence and implications of recent climate change in northern Alaska and other Arctic regions. Climatic Change 72 (3), 251–298.
Hinzman, L.D., Deal, C.J., McGuire, A.D., Mernild, S.H., Polyakov, I.V., Walsh, J.E., 2013. Trajectory of the Arctic as an integrated system. Ecol. Appl. 23, 1837–1868.
Holmgren, G.G., 1967. A rapid citrate-dithionite extractable iron procedure. Soil Sci. Soc. Am. Pro. 31, 210–211.
Kelly, S.D., Hesterberg, D., Ravel, B., 2008. Analysis of soils and minerals using X-ray absorption spectroscopy. In: Ulery, A.L., Drees, L.R. (Eds.), Methods of Soil Analysis. Part 5. Minerological Methods. Soil Science Society of America, Madison, pp. 378–463.
Kinsela, A.S., Jones, A.M., Bligh, M.W., Pham, A.N., Collins, R.N., Harrison, J.J., Wilsher, K.L., Payne, T.E., Waite, T.D., 2016. Influence of dissolved silicate on rates of Fe(II) oxidation. Environ. Sci. Technol. 50 (21), 11663–11671.
Lalonde, K., Mucci, A., Ouellet, A., Gélinas, Y., 2012. Preservation of organic matter in sediments promoted by iron. Nature 483 (7388), 198–200.
Linke, T., Gislason, S.R., 2018. Stability of iron minerals in Icelandic peat areas and transport of heavy metals and nutrients across oxidation and salinity gradients – a modelling approach. Energy Procedia 146, 30–37.
Lloret, E., Dessert, C., Gaillardet, J., Albéric, P., Crispi, O., Chatudeau, C., Benedetti, M. F., 2011. Comparison of dissolved inorganic and organic carbon yields and fluxes in the watersheds of tropical volcanic islands, examples from Guadeloupe (French West Indies). Chem. Geol. 280, 65–78.
Loeppert, R.H., Inskeep, W.P., 1996. Iron. In: Sparks, D.L., Page, A.L., Helmke, P.A., Loeppert, R.H., Soltanpour, P.N., Tabatabai, M.A., Johnston, C.T., Sumner, M.E. (Eds.), Methods of Soil Analysis, Part 3. Soil Science Society of America, Madison, Wisconson, Chemical Methods, pp. 639–644.
Malucelli, F., Terribile, F., Colombo, C., 1999. Mineralogy, micromorphology and chemical analysis of andosols on the Island of São Miguel (Azores). Geoderma 88 (1-2), 73–98.
Marin-Spiotta, E., Chadwick, O.A., Kramer, M., Carbone, M.S., 2011. Carbon delivery to deep mineral horizons in Hawaiian rain forest soils. J. Geophys. Res-Biogeo 116.
McKeague, J.A., 1967. An evaluation of 0.1 *M* pyrophosphate and pyrophosphate-dithionite in comparison with oxalate as extractants of accumulation products in podzols and some other soils Can. J. Soil Sci. 47, 95–99.
Mejia, J., Roden, E.E., Ginder-Vogel, M., 2016. Influence of oxygen and nitrate on Fe (hydr)oxide mineral transformation and soil microbial communities during redox cycling. Environ. Sci. Technol. 50 (7), 3580–3588.
Melton, E.D., Swanner, E.D., Behrens, S., Schmidt, C., Kappler, A., 2014. The interplay of microbially mediated and abiotic reactions in the biogeochemical Fe cycle. Nat. Rev. Microbiol. 12, 797–808.
Milliman, J.D., Syvitski, J.P.M., 1992. Geomorphic/tectonic control of sediment discharge to the ocean: The importance of small mountainous rivers. J. Geol. 100 (5), 525–544.
Ólafsson, H., Furger, M., Brümmer, B., 2007. The weather and climate of Iceland. Meteorol. Z. 16, 5–8.
Opfergelt, S., Burton, K.W., Georg, R.B., West, A.J., Guicharnaud, R.A., Sigfusson, B., Siebert, C., Gislason, S.R., Halliday, A.N., 2014. Magnesium retention on the soil exchange complex controlling Mg isotope variations in soils, soil solutions and vegetation in volcanic soils, Iceland. Geochim. Cosmochim. Acta 125, 110–130.
Opfergelt, S., Williams, H.M., Cornelis, J.T., Guicharnaud, R.A., Georg, R.B., Siebert, C., Gislason, S.R., Halliday, A.N., Burton, K.W., 2017. Iron and silicon isotope behaviour accompanying weathering in Icelandic soils, and the implications for iron export from peatlands. Geochim. Cosmochim. Acta 217, 273–291.
Óskarsson, H., Arnalds, Ó., Gudmundsson, J., Gudbergsson, G., 2004. Organic carbon in Icelandic Andosols: geographical variation and impact of erosion. Catena 56 (1-3), 225–238.
Parfitt, R.L., 1990. Allophane in New Zealand - A review. Aust. J. Soil Res. 28, 343–360.
Parfitt, R.L., Kimble, J.M., 1989. Conditions for formation of allophane in soils. Soil Sci. Soc. Am. J. 53, 971–977.
Pogge von Strandmann, P.A.E., James, R.H., van Calsteren, P., Gíslason, S.R., Burton, K. W., 2008. Lithium, magnesium and uranium isotope behaviour in the estuarine environment of basaltic islands. Earth Planet Sc. Lett. 274, 462–471.
Raudina, T.V., Loiko, S.V., Kuzmina, D.M., Shirokova, L.S., Kulizhskiy, S.P., Golovatskaya, E.A., Pokrovsky, O.S., 2021. Colloidal organic carbon and trace elements in peat porewaters across a permafrost gradient in Western Siberia. Geoderma 390, 114971.
Ravel, B., Newville, M., 2005. ATHENA, ARTEMIS, HEPHAESTUS: data analysis for X-ray absorption spectroscopy using IFEFFIT. J. Synchrotron Radiat. 12 (4), 537–541.
Rawlins, M.A., Steele, M., Holland, M.M., Adam, J.C., Cherry, J.E., Francis, J.A., Groisman, P.Y., Hinzman, L.D., Huntington, T.G., Kane, D.L., Kimball, J.S., Kwok, R., Lammers, R.B., Lee, C.M., Lettenmaier, D.P., McDonald, K.C., Podest, E., Pundsack, J.W., Rudels, B., Serreze, M.C., Shiklomanov, A., Skagseth, O., Troy, T.J., Vörösmarty, C.J., Wensnahan, M., Wood, E.F., Woodgate, R., Yang, D.Q., Zhang, K., Zhang, T.J., 2010. Analysis of the Arctic system for freshwater cycle intensification: Observations and expectations. J. Climate 23, 5715–5737.
Roden, E.E., Zachara, J.M., 1996. Microbial reduction of crystalline iron(III) oxides: Influence of oxide surface area and potential for cell growth. Environ. Sci. Technol. 30, 1618–1628.
Ryan, J.N., Gschwend, P.M., 1992. Effect of iron diagenesis on the transport of colloidal clay in an unconfined sand aquifer. Geochim. Cosmochim. Acta 56, 1507–1521.
Ryan, J.N., Gschwend, P.M., 1994. Effect of solution chemistry on clay colloid release from an iron oxide-coated aquifer sand. Environ. Sci. Technol. 28 (9), 1717–1726.
Senn, A.C., Kaegi, R., Hug, S.J., Hering, J.G., Mangold, S., Voegelin, A., 2015. Composition and structure of Fe(III)-precipitates formed by Fe(II) oxidation in water at near-neutral pH: Interdependent effects of phosphate, silicate and Ca. Geochim. Cosmochim. Acta 162, 220–246.

Smith, L.C., Sheng, Y., MacDonald, G.M. and Hinzman, L.D. (2005) Disappearing arctic lakes. Science 308, 1429-1429.

Stocker, T., Qin, D., Plattner, G.-K., Tignor, M., Allen, S., Boschung, J. and (Eds) (2013) Climate Change 2013: The physical science basis, Contribution of Working Group I to the Fifth Assessment Report of the Intergovernmental Panel on Climate Change. Cambridge University Press, Cambridge, United Kingdom, New York, NY, USA, p. 1535.

Su, C.M., Harsh, J.B., 1996. Alteration of imogolite, allophane, and acidic soil clays by chemical extractants. Soil Sci. Soc. Am. J. 60, 77–85.

ThomasArrigo, L.K., Mikutta, C., Byrne, J., Kappler, A., Kretzschmar, R., 2017. Iron(II)-catalyzed iron atom exchange and mineralogical changes in iron-rich organic freshwater flocs: An iron isotope tracer study. Environ. Sci. Technol. 51 (12), 6897–6907.

ThomasArrigo, L.K., Byrne, J., Kappler, A., Kretzschmar, R., 2018. Impact of organic matter on iron(II)-catalyzed mineral transformation in ferrihydrite-OM coprecipitates Environ. Sci. Technol. 52, 12316–12326.

ThomasArrigo, L.K., Kaegi, R., Kretzschmar, R., 2019. Ferrihydrite growth and transformation in the presence of ferrous Fe and model organic ligands. Environ. Sci. Technol. 53, 13636–13647.

ThomasArrigo, L.K., Bouchet, S., Kaegi, R., Kretzschmar, R., 2020. Organic matter influences transformation products of ferrihydrite exposed to sulfide. Env. Sci. Nano 7, 3405–3418.

ThomasArrigo, L.K., Notini, L., Shuster, J., Nydegger, T., Vontobel, S., Fischer, S., Kappler, A., Kretzschmar, R., 2022. Mineral characterization and composition of Fe-rich flocs from wetlands of Iceland: Implications for Fe, C and trace element export. Sci. Total Environ. 816, 151567.

Thompson, A., Chadwick, O.A., Boman, S., Chorover, J., 2006a. Colloid mobilization during soil iron redox oscillations. Environ. Sci. Technol. 40 (18), 5743–5749.

Thompson, A., Chadwick, O.A., Rancourt, D.G., Chorover, J., 2006b. Iron-oxide crystallinity increases during soil redox oscillations. Geochim. Cosmochim. Acta 70 (7), 1710–1727.

Thompson, A., Rancourt, D.G., Chadwick, O.A., Chorover, J., 2011. Iron solid-phase differentiation along a redox gradient in basaltic soils. Geochim. Cosmochim. Acta 75, 119–133.

Torn, M.S., Trumbore, S.E., Chadwick, O.A., Vitousek, P.M., Hendricks, D.M., 1997. Mineral control of soil organic carbon storage and turnover. Nature 389 (6647), 170–173.

Van Groeningen, N., ThomasArrigo, L.K., Byrne, J.M., Kappler, A., Christl, I., Kretzschmar, R., 2020. Interactions of ferrous iron with clay mineral surfaces during sorption and subsequent oxidation. Environ. Sci-Proc. Imp. 22, 1355–1367.

Vepraskas, M.J., Polizzotto, M.L., Faulkner, S.P., 2016. Redox Chemistry of Hydric Soils. In: Vepraskas, M.J., Craft, C.B. (Eds.), Wetland Soils: Genesis, Hydrology, Landscapes, and Classification. CRC Press: Taylor and Francis Group, New York, pp. 105–132.

Vogelsang, V., Kaiser, K., Wagner, F.E., Jahn, R., Fiedler, S., 2016. Transformation of clay-sized minerals in soils exposed to prolonged regular alternation of redox conditions. Geoderma 278, 40–48.

Wilmoth, J.L., Moran, M.A., Thompson, A., 2018. Transient O_2 pulses direct Fe crystallinity and Fe(III)-reducer gene expression within a soil microbiome. Microbiome 6, 1–14.

Winkler, P., Kaiser, K., Thompson, A., Kalbitz, K., Fiedler, S., Jahn, R., 2018. Contrasting evolution of iron phase composition in soils exposed to redox fluctuations. Geochim. Cosmochim. Acta 235, 89–102.

WRB, I.W.G. (2014) World Reference Base for Soil Resources 2014. International soil classification system for naming soils and creating legends for soil maps. FAO, Rome.

Ye, C.L., Hall, S.J., Hu, S.J., 2019. Controls on mineral-associated organic matter formation in a degraded Oxisol. Geoderma 338, 383–392.

Zhou, Z., Latta, D.E., Noor, N., Thompson, A., Borch, T., Scherer, M.M., 2018. Fe(II)-catalyzed transformation of organic matter-ferrihydrite coprecipitates: A closer look using Fe isotopes. Environ. Sci. Technol. 52 (19), 11142–11150.